RSC Advances

PAPER

View Article Online
View Journal | View Issue

Cite this: *RSC Adv.*, 2020, **10**, 4512

Different agglomeration properties of $PC_{61}BM$ and $PC_{71}BM$ in photovoltaic inks – a spin-echo SANS study†

Gabriel Bernardo, *[a] Manuel Melle-Franco, [b] Adam L. Washington, [c] Robert M. Dalgliesh, [c] Fankang Li, [d] Adélio Mendes [a] and Steven R. Parnell*[e]

Received 2nd October 2019
Accepted 10th December 2019

DOI: 10.1039/c9ra08019h

rsc.li/rsc-advances

Fullerene derivatives are used in a wide range of applications including as electron acceptors in solution-processable organic photovoltaics. We report agglomeration of fullerene derivatives in optically opaque solutions of $PC_{61}BM$ and $PC_{71}BM$, with concentrations ranging from 30 mg mL^{-1} up to 90 mg mL^{-1}, in different solvents with relevance to organic photovoltaics, using a novel neutron scattering technique, Spin-Echo Small Angle Neutron Scattering (SESANS). From SESANS, agglomerates with correlation lengths larger than 1 μm are found in some $PC_{61}BM$ solutions, in contrast no agglomerates are seen in $PC_{71}BM$ solutions. These results clearly show that $PC_{71}BM$ is fundamentally more soluble than $PC_{61}BM$ in the solvents commonly used in photovoltaic inks and corroborating similar observations previously achieved using other experimental techniques. Computer models are presented to study the energetics of solution and agglomeration of both species, ascribing the difference to a kinetic effect probably related to the larger anisotropy of $PC_{71}BM$. Also, this work showcases the power of SESANS to probe agglomerates of fullerene derivatives in completely opaque solutions for agglomerates of the order of one to several microns.

1. Introduction

Fullerene derivative [6,6]-phenyl-C61-butyric acid methyl ester ($PC_{61}BM$) and its analogue [6,6]-phenyl-C71-butyric acid methyl ester ($PC_{71}BM$) are the two most widely used electron-accepting materials in organic photovoltaics (OPVs).[1,2] A key difference between $PC_{61}BM$ and $PC_{71}BM$ is the ellipsoidal shape of the latter as compared to the more spherical $PC_{61}BM$ molecule.[3] The lower symmetry and more extended conjugation of C_{70} enable energetic transitions that are forbidden in C_{60}, leading to a broader photo-absorption profile of the corresponding derivatives in the visible region of the solar spectrum.[4] This allows increased photon harvesting, and a potentially higher photocurrent for devices using $PC_{71}BM$ rather than $PC_{61}BM$, an important attribute that has brought the C_{70} analogue to the forefront of OPV research (despite its higher cost). The energy levels and good electron mobility of $PC_{71}BM$ also enable it to be used as an electron transport layer in perovskite solar cells.[5–7]

The manufacturing of organic photovoltaic devices relies on the use of solution-processing methods such as spin-coating, spray coating and inkjet printing. Therefore, to be processed during device manufacture, fullerene-based acceptors need to have a reasonably high solubility in a given solvent. Chlorobenzene, toluene and chloroform are typical solvents used in film deposition of blends of fullerene derivatives and conjugated polymers, commonly known as bulk-heterojunction (BHJ), during the laboratory scale production of OPV devices. The relative solubility of the fullerene-based acceptors in the photovoltaic ink solution influences their precipitation behaviour during thin film processing, playing therefore a crucial role in the morphology of the BHJs and consequently in the corresponding device performances.[8–11] Besides the use of different processing solvents, another approach to control the morphology of BHJs and the corresponding device performance consists in adding to the photovoltaic ink solution small amounts (typically 3% v/v) of a high boiling point additive, 1,8-diiodooctane (DIO) being the most popular one.[12–15]

The solubility and agglomeration[16] behaviour of different fullerenes and fullerene derivatives in organic solvents and additives, with relevance for photovoltaic applications, has been the subject of significant research in the two last decades.[17]

[a]*LEPABE – Laboratory for Process Engineering, Environment, Biotechnology and Energy, Faculty of Engineering, University of Porto, Rua Dr Roberto Frias, 4200-465 Porto, Portugal. E-mail: gbernardo@fe.up.pt*

[b]*CICECO—Aveiro Institute of Materials, Department of Chemistry, University of Aveiro, 3810-193 Aveiro, Portugal*

[c]*ISIS Pulsed Neutron and Muon Source, STFC, Rutherford Appleton Laboratory, Harwell, Oxon, OX11 0QX, UK*

[d]*Neutron Technologies Division, Oak Ridge National Laboratory, Oak Ridge, TN 37830, USA*

[e]*Faculty of Applied Sciences, Delft University of Technology, Mekelweg 15, 2629 JB Delft, Netherlands. E-mail: S.R.Parnell@tudelft.nl*

† Electronic supplementary information (ESI) available. See DOI: 10.1039/c9ra08019h

Studies of C_{60},[18–31] C_{70},[29,32–34] $PC_{61}BM$,[2,23–26,35–40] $PC_{71}BM$[2,14,15,38,41–43] and others[2,26,44,45] in various organic solvents, were performed using an array of techniques. These include high-performance liquid chromatography (HPLC),[2] optical absorption,[32–34] fluorescence spectroscopy,[32,33] static/dynamic light scattering at $\lambda > 700$ nm,[18,19,22,32,33] positron lifetime spectroscopy,[20,27] electron microscopy,[22,32] small-angle neutron scattering (SANS),[14,15,44–46] small-angle X-ray scattering (SAXS)[22,45,46] and theoretical calculations (molecular dynamics simulations, *ab initio* DFT, and others).[23–26,35,47–49] Despite all these studies, the reports on the solubility and agglomeration of $PC_{71}BM$ and its comparison with $PC_{61}BM$ are still scarce[2,3] and there is in some cases a large discrepancy amongst the solubility values reported by different authors, as shown in Table 1. The most detailed comparison between the solubilities of both fullerene derivatives was performed by Kronholm *et al.*[2] who published solubility values, determined by HPLC analysis of the liquid phase at room temperature, for $PC_{61}BM$ and $PC_{71}BM$ in different organic solvents, including chlorobenzene, toluene and chloroform. For both $PC_{61}BM$ and $PC_{71}BM$, the highest solubility was found with chlorobenzene and chloroform (each 25 mg mL^{-1}) and the lowest solubility with toluene (<20 mg mL^{-1}). Importantly, $PC_{71}BM$ was found to be in all cases more soluble than $PC_{61}BM$. Williams *et al.*[3] compared the properties of $PC_{61}BM$ with $PC_{71}BM$ using molecular dynamics simulations coupled with electronic structure calculations. They concluded that although $PC_{71}BM$ should have similar compatibility with solvents as $PC_{61}BM$, increased solubility of $PC_{71}BM$ can arise due to the increased volume and surface area of the ellipsoidal shape.

Fullerenes and fullerene derivatives, due to their high C/H ratio and high density, possess neutron scattering lengths very different from normal hydrogenous organic compounds and therefore no deuteration of one or more components is needed to obtain good neutron contrast between them (see Table S1 in ESI†[50]). For this reason, neutron scattering techniques are particularly well suited for studying their agglomeration in hydrogenous organic matrices and have been previously used in the study of agglomeration in BHJ solar cells[12,51,52] and in organic solvents.[44,45,53–56] In the particular case of neutron scattering studies of fullerenes and functionalized fullerenes in organic solvents, SANS has been used both in the Guinier and Porod regimes, namely: (i) Guinier regime in the measurement of the radius of gyration (R_g) of well dissolved individual C_{60} and C_{70} molecules in undersaturated solutions with no measurable fullerene–fullerene interactions[53–55] and (ii) Porod regime in the study of colloidal suspensions of C_{60} agglomerates in CS_2 (ref. 55) and water[56] and agglomerates of functionalized-C_{60} (with large pendant alkyl groups) in hexane-d_{14}.[44,45] Essentially, for any neutron scattering technique to show scattering, it is necessary to have distinct interfaces at the length scales which are being probed and sufficient contrast, to observe them. Hence, any well dissolved material will have low or little scattering at the length scales probed and therefore no observable signal is detected in either SANS or SESANS. Moreover, as we will show below, due to SESANS measuring in polarisation in absolute units it is relatively simple to relate the observed scattering directly to a volume fraction of agglomerate.

SESANS is a relatively new technique able to measure bulk buried structures over 3 orders of magnitude in length scale, from *ca.* 50 nm to 20 μm. This is two orders of magnitude larger than conventional SANS, which covers length scales from *ca.* 1 nm to 200 nm. SESANS is comparable to what may be studied with light scattering (LS) though with the complementary benefits afforded by the use of neutrons such as contrast and the ability to probe the bulk of opaque solutions with virtually 0% optical transmission. In these measurements, SESANS is implemented using a series of radio frequency (RF) coils and shaped magnetic fields used to encode the scattering angle in the spin precession of a beam of polarised neutrons.[57] Neutrons scattered through different angles traverse magnetic fields of different lengths and thus precess by a different amount to the unscattered neutrons and hence changes the measured polarisation. The measured quantity is the polarisation measured with a sample (P_S) corrected for polarisation without a sample (P_0). Full details are presented in ESI† along with the relevant theory. SESANS has found some recent practical applications in materials science, for instance in the study of fullerene agglomerates in polymer composites[58,59] and the porosity of silica Stöber particles.[60]

In this work, we describe the first application of SESANS to the study of the agglomeration behaviour of the functionalized fullerenes $PC_{61}BM$ and $PC_{71}BM$ in different organic solvents, with relevance to organic photovoltaics. In particular, we studied $PC_{61}BM$ and $PC_{71}BM$ agglomeration behaviour in solutions with concentrations 30, 60 and 90 mg mL^{-1} and based on the solvents chlorobenzene, toluene and chloroform as well as in DIO, a common additive in the preparation of OPV inks.[61]

Table 1 Solubility values (mg mL^{-1}), measured at 25 °C, of $PC_{61}BM$ and $PC_{71}BM$ in different solvents, as reported in the literatures[a]

	Solubility (mg mL^{-1})	
	$PC_{61}BM$	$PC_{71}BM$
Chloroform	25[a], 27[e], 28.8[c]	30[a], 61.1[e]
Toluene	10[a], 10.9[e], 15.6[c], 19[d]	20[a], 27.4[e]
Chlorobenzene	25[a], 35[f], 37.1[e], 39.4[g], 45[d], 50[b], 59.5[c]	40[a], 60.6[e], 80[b], 207[h]
DIO	24[f]	21.7[i], 35[j]

[a] [a]Ref. 2; [b]ref. 8; [c]ref. 10; [d]ref. 23; [e]ref. 38; [f]ref. 39; [g]ref. 40; [h]ref. 41; [i]ref. 42; [j]ref. 43.

Even though these $PC_{61}BM$ and $PC_{71}BM$ concentrations are higher than those normally used in the preparation of OPV devices, this study is of particular relevance to the understanding of fullerene derivative ($PC_{61}BM$ and $PC_{71}BM$) agglomeration, triggered by solvent evaporation, during the process of bulk-heterojunction thin film drying.[62–64] In devices processed with DIO, after active layer deposition, DIO evaporates much slower than the main solvent,[12] and this justifies the relevance of our study of agglomeration also in concentrated DIO solutions.

2. Materials and methods

Fullerene derivatives $PC_{61}BM$ (empirical formula $C_{72}H_{14}O_2$ and $M_w = 910.88$ g mol^{-1}) and $PC_{71}BM$ (empirical formula $C_{82}H_{14}O_2$ and $M_w = 1030.99$ g mol^{-1}), both with >99% purity, were purchased from Solenne BV, and their chemical structure is shown in Fig. 1. The additive DIO 97+% was purchased from Alfa Aesar. Chloroform (puriss p.a. > 99%), toluene (ACS reagent ≥ 99.5%) and chlorobenzene (ACS reagent, ≥99.5%) were purchased from Sigma-Aldrich.

Sample solutions (0.7 mL) of $PC_{61}BM$ and $PC_{71}BM$ with concentrations 30, 60 and 90 mg mL^{-1} were prepared in four different solvents (chlorobenzene, toluene, chloroform and DIO) by weighting the appropriate amounts of fullerene derivatives and measuring the appropriate volumes of solvents into amber glass vials with 2 mL volume and screw cap. Then the solutions were stirred vigorously in a hot plate at 80 °C (except chloroform solutions which, due to their high volatility, were stirred at room temperature) for approximately 3 hours. After cooling down to room temperature the solutions were transferred into disc-shaped "banjo" quartz cells with a 1 mm pathlength and an approximate volume of 0.7 mL and these were transferred into the beamline. The measurements were taken on the Larmor instrument[65] at the ISIS Pulsed Neutron and Muon source. Larmor is a new instrument which can be configured in both SANS and SESANS modes.

During measurements, to guarantee that the solutions remained macroscopically as homogeneous as possible, the banjo cells were continuously rotated (∼6 rpm) using a home-made rotation apparatus with cell holders made of Teflon (non-magnetic material) specially build for this purpose, Fig. S1.† SESANS measurements were taken at −20°, −50° and −75° magnet angles with neutron wavelengths of 2.75 to 10 Å. These settings correspond to the following spin echo length ranges: 1–13.5 μm, 0.36–4.75 μm and 0.13–1.67 μm. Also, the data was truncated at long spin echo lengths whenever the polarisation dropped below 0.1. In some cases, where scattering was not observed, we report only the results for the −20° angle.

Computer calculations of $PC_{61}BM$ and $PC_{71}BM$, as well as of C_{60} and C_{70} as a reference, were performed first with a novel semiempirical quantum mechanics Hamiltonian[66] and then at the DFT M06-2X-6-31g(d,p) Hamiltonian with continuum solvation models. Similar results were obtained for both models and only DFT results will be reported. With DFT, we optimized the molecular geometry of one molecule of $PC_{61}BM$ and $PC_{71}BM$ and their dimers in a continuum of toluene in cartesian space starting from the molecular conformations of high-quality crystallographic data.[67,68] Then, the free solvation energies corrections in toluene, chlorobenzene and chloroform were computed with a molecular cavity corrected by an additional central sphere of 0.5 Å sitting on the geometric center of each fullerene, C_{60}/C_{70}, moiety with the SMD methodology. The correction was added after we found that, with the default parameters, GePOL generated molecular cavities presented an unphysical solvent filled volume in the fullerenes center. The computed quantities represent the free energy required to transfer a molecule from the gas phase to a solution at the limit of infinite dilution. All calculations were done by Gaussian 09.[69]

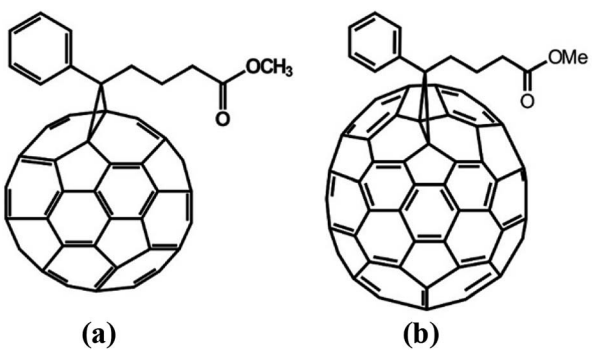

Fig. 1 Chemical structures of $PC_{61}BM$ (a) and $PC_{71}BM$ (b).

3. Results and discussion

Qualitatively, a full range of behaviours is obtained for $PC_{61}BM$ solutions from SESANS, Fig. 2. While some of the "solutions" scatter strongly (*e.g.* $PC_{61}BM$ in DIO at 90 mg mL^{-1}), others scatter weakly (*e.g.* $PC_{61}BM$ in $CHCl_3$ at 60 mg mL^{-1}) and others do not scatter at all (*e.g.* $PC_{61}BM$ in DIO at 30 mg mL^{-1}). In comparison, none of the $PC_{71}BM$ solutions scatter, Fig. 3(a). This is clear indication that $PC_{71}BM$ is fundamentally more soluble than $PC_{61}BM$ in the solvents considered, agreeing with results determined using other techniques, Table 1.

For each SESANS measurement, we plot the 'normalised SESANS signal'.[70,71] Qualitatively this can be interpreted as a correlation function $G(z)$ related to a Debye type correlation function. At long spin-echo lengths $G(z \rightarrow \infty)$ the value of this normalised spin-echo signal is given by Σ_t and this can be converted directly to a volume fraction when scattering is observed. Hence, for the samples where the normalised spin-echo signal is ∼0 it can be stated that the functionalized fullerene molecules are completely molecularly dissolved or in the case of existing agglomerates in solution these are either too large and beyond the accessible length scale of the technique, *i.e.* tens of microns in size, or are present in very small quantities below the detection limit of the technique. By contrast, for the samples where the normalised spin-echo signal is ≠0, there is clear agglomeration behaviour on the micrometer length scale (*cf.* $PC_{61}BM$ in DIO at 60 and 90 mg mL^{-1}). Following the formalism of Andersson *et al.*[72] it is possible to adapt the standard libraries of form and structure factors utilized in

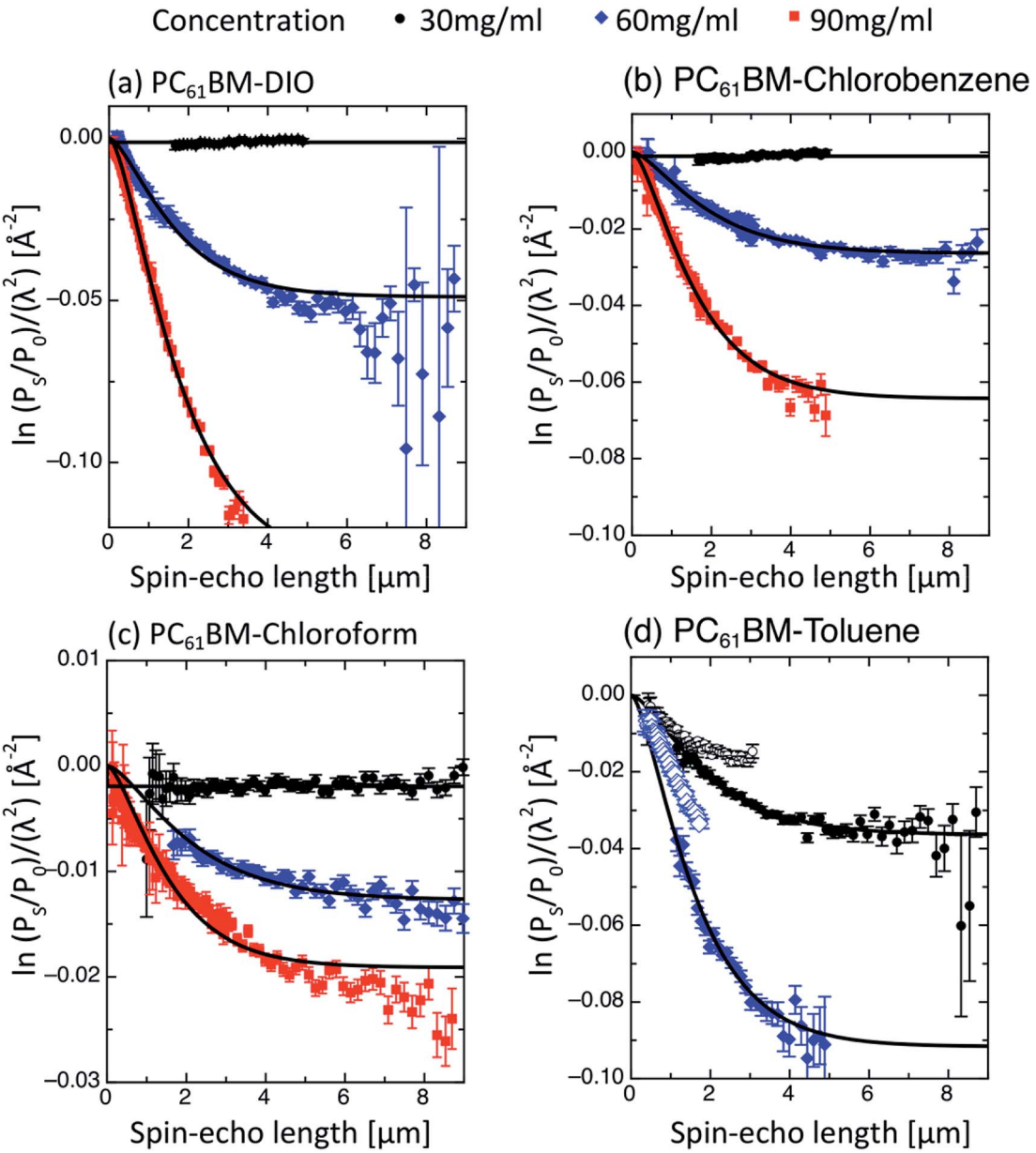

Fig. 2 Normalised SESANS signals of $PC_{61}BM$ solutions as a function of the spin echo length, in the following solvents: (a) DIO, (b) chlorobenzene, (c) chloroform and (d) toluene with the concentrations denoted on the legend at the top. Note that in the case of the toluene the open symbols are measurements at a pole shoe angle of −50° and at an earlier time than the closed symbol measurements at −20°.

conventional SANS for using with SESANS. Both a hard sphere and the Debye–Anderson–Brumberger (DAB)[73,74] model were applied and the better agreement was found using the DAB model. The DAB model makes no assumptions concerning the underlying structure of the agglomerates and calculates the scattering from a randomly distributed, two-phase system that is characterized by a single length scale – the correlation length, a – which is a measure of the average spacing between regions of the two different phases (1 and 2). The DAB model has an exact form for $G(z)$, as shown in Fig. 3(b) and in ESI,† and the resulting DAB fitting parameters are shown in Table 2 along with the derived volume fractions of each phase, calculated using the scattering length density values of the pure components. For some systems only a depolarisation is observed and in this case it is not possible to fit a defined length scale thus indicated by n/a. As the observed characteristic length scale is broadly of the order of ∼1 μm and similar for the various concentrations then we use the value to extract a volume fraction using the length scale obtained for the higher concentration.

The solutions of $PC_{61}BM$ in toluene (Fig. 2(d)) are very unstable as an evolution of agglomeration can be seen during the time of the measurement (∼2 h). Specifically, the two branches of the scattering curve corresponding to different spin-echo lengths do not overlap with each other. For this reason, in these $PC_{61}BM$–toluene systems, only the part of the

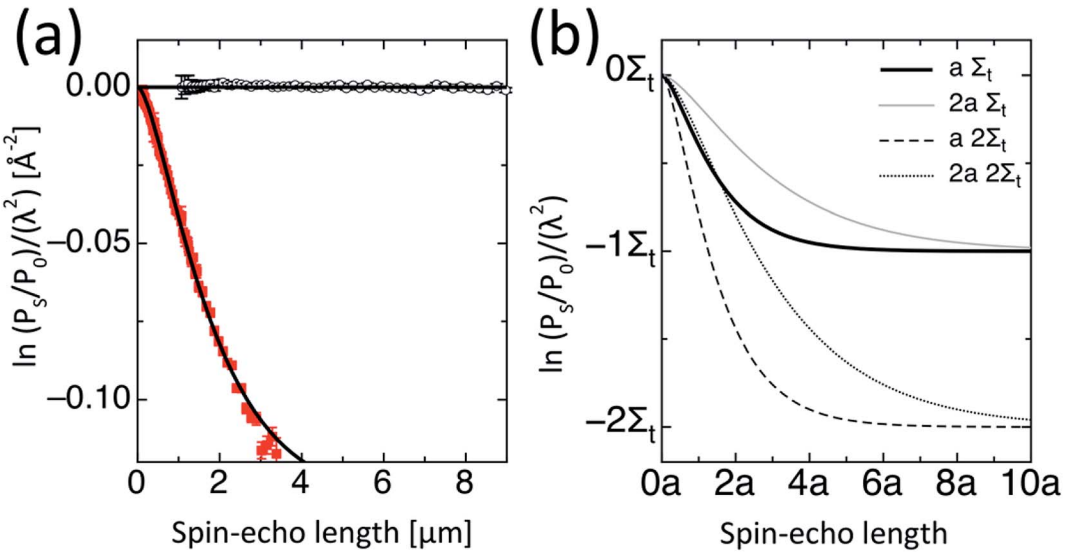

Fig. 3 (a) Representative example of the SESANS data, showing a normalized spin-echo signal ~ 0 ($PC_{71}BM$ 90 mg mL^{-1} in DIO), obtained with all the tested $PC_{71}BM$ solutions. The spin-echo signal for the corresponding $PC_{61}BM$ solution (90 mg mL^{-1} in DIO) is also shown for comparison. (b) Simulated reduced SESANS signal for the DAB model for different correlation lengths *a* and multiples of the saturation value Σ_t. This illustrates the two pieces of information on the correlation lengths observed and the total scattering. The length scale *a* determines the spin-echo length at which the curves plateau and Σ_t gives the saturation level obtained at long spin-echo length.

scattering curves corresponding to magnet angles of −20° has been fitted, with which the setup can access the longest and broadest length scale. These results also suggest that toluene is the worst solvent of the series for $PC_{61}BM$, as the $PC_{61}BM$–toluene solution is the only one that scatters at its lowest concentration (30 mg mL^{-1}), which indicates the presence of local scattering centers. This is in qualitative agreement with previous solubilities determined by other techniques, Table 1, which also finds that toluene is the worst solvent of this series for $PC_{61}BM$. Concerning the solutions of $PC_{61}BM$ in chloroform, chlorobenzene and DIO, the volume fraction of agglomerated $PC_{61}BM$ increases with concentration as expected, Table 2. In these oversaturated solutions measured immediately after preparation, the average size of the agglomerates is in the range from 1.1 to 1.5 μm. Interestingly, the agglomerate size appears to decrease with increasing bulk concentration for every solvent (except DIO). A likely reason is that at higher concentrations and under the stirring rotation conditions used in the measurements, there is more chance for collisions to occur between agglomerates. As the agglomerates are formed by loosely bound $PC_{61}BM$ molecules, it is possible that some fragmentation and erosion of the agglomerates may occur with a consequent reduction in their average dimensions. Also surprisingly, in toluene and chlorobenzene the solubility apparently decreases with increasing solute concentration, which might be due to a kinetic effect, the depletion of the bulk concentration being more rapid when there is more agglomeration.

In the $PC_{61}BM$ solutions in chloroform, chlorobenzene and DIO, no evolution of agglomeration was observed during the time of the SESANS experiment (~2 hours). However, a clear macroscopic phase segregation was visible with naked eye, in

Table 2 SESANS fitting parameters calculated using the DAB model

Solvent	$PC_{61}BM$ concentration (mg mL^{-1})	$\frac{\sum_t}{\lambda^2}$ ($Å^{-2}$)	Φ_{PCBM} (aggl.)	DAB – correlation length [μm]	Solubility (mg mL^{-1})
$CHCl_3$	30	$1.8 \times 10^{-3} \pm 1.5 \times 10^{-3}$	0.0016	n/a	—
	60	$1.27 \times 10^{-2} \pm 2.06 \times 10^{-4}$	0.012	1.45 ± 0.06	42
	90	$1.91 \times 10^{-2} \pm 1.67 \times 10^{-4}$	0.023	1.08 ± 0.02	55.5
Toluene	30 (20°)	$3.63 \times 10^{-2} \pm 5 \times 10^{-4}$	0.012	1.32 ± 0.04	12
	60 (20°)	$1.04 \times 10^{-5} \pm 1.47 \times 10^{-7}$	0.037	1.11 ± 0.03	4.5
Chlorobenzene	30	$1.02 \times 10^{-3} \pm 6.5 \times 10^{-4}$	0.0006	n/a	—
	60	$2.64 \times 10^{-2} \pm 2.3 \times 10^{-4}$	0.016	1.30 ± 0.02	36
	90	$6.43 \times 10^{-2} \pm 6 \times 10^{-4}$	0.048	1.10 ± 0.01	18
DIO	30	1.16×10^{-3}	0.0002	n/a	—
	60	$4.89 \times 10^{-2} \pm 4.0 \times 10^{-4}$	0.012	1.14 ± 0.04	42
	90	$0.13 \pm 1.4 \times 10^{-3}$	0.031	1.23 ± 0.01	43.5

most of the solutions, after being at rest for ~48 hours after the experiment (Fig. S2†). It must be noted that the kinetics of agglomeration of $PC_{61}BM$ in different solvents is dictated not only by the corresponding thermodynamic solubilities but also by the density differences (Table S1†) between the solvent and the fullerene derivative. In particular, the fast kinetics of agglomeration observed in toluene is in part due to the large density difference between toluene (0.87 g cm^{-3}) and $PC_{61}BM$ (1.5 g cm^{-3}). The fact that no $PC_{71}BM$ solutions displayed any noticeable phase segregation in the same conditions, namely after being ~48 h at rest, indicates a fundamental difference between both systems.

The phase segregation observed in most $PC_{61}BM$ solutions, after 48 h at rest, shows that our SESANS results obtained in fresh solutions, and the derived values of solubilities (Table 2), do not represent fully equilibrated systems due to the slow agglomeration kinetics. Consequently, the presented values are not true thermodynamic solubilities but are qualitative indicators of how easily the two functionalized fullerenes can be dissolved in the four different solvents under the experimental conditions considered. In fact, for most of the $PC_{61}BM$ solutions, there is a slow and continuous agglomeration of the fullerene derivatives which can only be detected visually after days.

The SANS signal for some of the solutions in the banjo cells was also measured, under rotation using the same experimental setup described above (Fig. S1†). The SANS data obeys a power law relationship with a slope of q^{-4} which points to the presence of sharp solution–agglomerate interfaces, Fig. S3.† However, it must be noted that these measurements were performed ~5 days after the SESANS measurements and due to the kinetics involved some further agglomeration should have occurred.

Computer DFT models were used to explore the fundamental interactions of $PC_{61}BM$ and $PC_{71}BM$ in different solvents. Three solvents, namely: toluene, chlorobenzene and chloroform were studied yielding similar results, Table 3. When compared, the computed solvation energies are quite similar for the three solvents, as it would be expected due to the similar dielectric constants. As a reference, C_{60} and C_{70} solvation free energies were also computed and compared with experimental values. Interestingly, although the absolute values differ, the trends with available data match almost quantitatively which serves to validate the approach used. Namely, the difference in solvation free energy of C_{70} and C_{60}, in toluene, −3.9 kcal mol^{-1}, is predicted to be −5.7 kcal mol^{-1} by the model, also the difference in solvation free energy of C_{60} in chlorobenzene and toluene, −0.6 kcal mol^{-1}, while the computed value is −1.1 kcal mol^{-1}.

Generally, for all the systems studied, solvation in a solvent continuum is predicted computationally to be exergonic with larger values for the functionalized fullerenes with respect to their pristine counterparts. Interestingly, a similar trend is obtained when compared, C_{70} *vs.* C_{60} and $PC_{71}BM$ *vs.* $PC_{61}BM$, the larger fullerene shows larger solvation energies in excess of 5.2–6.1 kcal mol^{-1} in both cases which is similar in value to the 4 kcal mol^{-1} extra solvation energy measured for C_{70} in toluene. This quantity only corresponds to an increase of the free energy of solvation of 12–15% which we believe it is too modest to account for the fundamental agglomeration difference observed experimentally.

In order to further explore this matter, we also computed the binding energy for $PC_{71}BM$ and $PC_{61}BM$ dimers in the three solvent studies to quantify, if approximately, the potential energy contribution behind the agglomeration phenomena. The dimerization energy was found to be very similar for the three solvents, between 6.6 and 7.5 kcal mol^{-1} and virtually the same for $PC_{71}BM$ and $PC_{61}BM$ for each solvent, Table 4. This finding indicates, that unsurprisingly, the enthalpic contribution to the agglomeration is probably similar for both systems, $PC_{71}BM$ and $PC_{61}BM$, and that the difference observed in agglomeration should be due to substantial dynamic effects, whose study are not feasible with the models presented.

In contrast, the dynamics of C_{60} and $PC_{61}BM$ in organic solvents were studied by Wang and Hua using molecular dynamics with a classical force field.[23] This study reported that the large enhancements of solubility found for $PC_{61}BM$ with respect to C_{60} correlates with the dynamics of the first solvation shell. In addition, solubility was found to correlate with the $PC_{61}BM$ reorientation velocity, and this is slowed down considerably due to the anisotropy of these molecules which probably hampers their agglomeration increasing the solubility with respect to C_{60}. Interestingly, this computational result justifies the slow agglomeration phenomena observed in our $PC_{61}BM$ experiments. Based on these observations, we propose, that the larger anisotropy of $PC_{71}BM$, with an ellipsoidal fullerene moiety, with respect to $PC_{61}BM$, with a spherical fullerene moiety, plays an important role in the decreased agglomeration and, consequently, in the enhanced solubility of $PC_{71}BM$ with respect to $PC_{61}BM$.

Finally, we make some comments about the advantages of SESANS for measuring the solubility of fullerenes and fullerene

Table 3 Computed and measured solution free energies of C_{60}, C_{70}, $PC_{61}BM$ and $PC_{71}BM$ in chloroform, toluene and chlorobenzene[a]

Solvent	Method	C_{60}	C_{70}	Diff. C_{70}–C_{60}	$PC_{61}BM$	$PC_{71}BM$	Diff. $PC_{71}BM$–$PC_{61}BM$
Chloroform	DFT	−32.1	−37.7	−5.6	−39.7	−45.0	−5.2
Toluene	DFT	−34.0	−39.6	−5.7	−40.0	−45.4	−5.3
Toluene	Exp.	−28.8	−32.8	−3.9	—	—	—
Chlorobenzene	DFT	−35.0	−41.2	−6.1	−43.1	−48.9	−5.8
Chlorobenzene	Exp.	−29.4	—	—	—	—	—

[a] Experimental data from ref. 75. All energies in kcal mol^{-1}.

Table 4 Binding energies for $PC_{61}BM$ and $PC_{71}BM$ dimers computed with different solvent continua based on M06-2X-Toluene-6-31g(d,p) molecular geometries[a]

	Dimer	
	Binding energy	
Solvent	$PC_{61}BM$	$PC_{71}BM$
Chloroform	−7.5	−7.2
Toluene	−7.1	−7.2
Chlorobenzene	−6.6	−6.6

[a] All energies in kcal mol^{-1}.

derivatives in organic solvents compared to the standard procedures. The common procedure used is very tedious and time-consuming and usually involves the following steps: (i) production of a calibration curve from the UV-Vis absorption spectra of diluted solutions of known concentrations; (ii) preparation of saturated solutions by stirring an excess of solid material with a small volume of test solvent; (iii) filtration or centrifugation of the saturated solutions so as to remove all the undissolved solid material; (iv) dilution of the solid-free saturated solutions with excess solvent in order to achieve an optical density within the range of the calibration curves determined in (i); (v) determination of a diluted concentration value and multiplication by the dilution factor employed. Compared with this standard procedure, SESANS is very advantageous because it only requires the step (ii) and it is able to determine *in situ* the presence or absence of agglomerates and therefore it avoids the tedious processes of filtration/centrifugation and dilution to the optical density of previously determined calibration curves.

4. Conclusions

In conclusion, the novel neutron scattering technique SESANS, has been used to study the agglomeration behaviour of the fullerene derivatives $PC_{61}BM$ and $PC_{71}BM$ in different solvents relevant for organic photovoltaics. Remarkably, large agglomerates with sizes in the range 1.1 to 1.5 μm were observed in freshly prepared $PC_{61}BM$ solutions, while such agglomerates were completely absent in $PC_{71}BM$ solutions of identical concentration. These results indicate clearly and unambiguously that $PC_{71}BM$ is kinetically more stable in solution than $PC_{61}BM$. Although we were able to estimate solubility values from the scattering of freshly prepared solutions, these values should be considered indicative due to the posterior detection of agglomeration in most $PC_{61}BM$ solutions. Computer DFT models show that, as intuitively expected, the $PC_{61}BM$ and $PC_{71}BM$ are fundamentally similar and consequently we argue that their differences in solvation free energy are unlikely to be responsible for the behaviour observed. In addition, we postulate that the differences observed are due to slower kinetics hampering agglomeration due to the larger molecular anisotropy of $PC_{71}BM$ with respect to $PC_{61}BM$. More generally, this work showcases the use of SESANS to directly probe particle agglomeration in dark opaque solutions, quite common with carbon-based nanomaterials and molecules, such as the case of highly concentrated fullerene and fullerene derivative solutions. A detailed SESANS study of the kinetics of agglomeration in these systems is planned and will be addressed in the future.

Conflicts of interest

None.

Acknowledgements

We thank Dr Stephen King (ISIS/STFC) for very useful discussions. We thank STFC (UK) and NWO (Netherlands) for the funding of beamtime for these experiments (Experiment RB1720483 – https://doi.org/10.5286/ISIS.E.92924123) and J. Plomp (TU Delft) for assistance with the design and implementation of the sample rotator used in these experiments. This work was financially supported by: Base Funding – UIDB/00511/2020 of the Laboratory for Process Engineering, Environment, Biotechnology and Energy – LEPABE – funded by national funds through the FCT/MCTES (PIDDAC). MMF acknowledges support from the Portuguese Foundation for Science and Technology (FCT), under the projects PTDC/FIS-NAN/4662/2014, IF/00894/2015, and FCT Ref. UID/CTM/50011/2019 for CICECO – Aveiro Institute of Materials.

References

1 C. Z. Li, H. L. Yip and A. K. Y. Jen, Functional fullerenes for organic photovoltaics, *J. Mater. Chem.*, 2012, **22**(10), 4161–4177.
2 D. Kronholm and J. C. Hummelen, Fullerene-Based n-Type Semiconductors in Organic Electronics, *Mater. Matters*, 2007, **2**(3), 16–20.
3 M. Williams, *et al.*, Influence of Molecular Shape on Solid-State Packing in Disordered $PC_{61}BM$ and $PC_{71}BM$ Fullerenes, *J. Phys. Chem. Lett.*, 2014, **5**(19), 3427–3433.
4 F. Zhang, *et al.*, Influence of $PC_{60}BM$ or $PC_{70}BM$ as electron acceptor on the performance of polymer solar cells, *Sol. Energy Mater. Sol. Cells*, 2012, **97**, 71–77.
5 G. Yang, *et al.*, Recent progress in electron transport layers for efficient perovskite solar cells, *J. Mater. Chem. A*, 2016, **4**(11), 3970–3990.
6 K. Mahmood, S. Sarwar and M. T. Mehran, Current status of electron transport layers in perovskite solar cells: materials and properties, *RSC Adv.*, 2017, **7**(28), 17044–17062.
7 T. Gatti, *et al.*, The Renaissance of fullerenes with perovskite solar cells, *Nano Energy*, 2017, **41**, 84–100.
8 P. A. Troshin, *et al.*, Material Solubility-Photovoltaic Performance Relationship in the Design of Novel Fullerene Derivatives for Bulk Heterojunction Solar Cells, *Adv. Funct. Mater.*, 2009, **19**(5), 779–788.
9 P. A. Troshin, *et al.*, Material solubility and molecular compatibility effects in the design of fullerene/polymer composites for organic bulk heterojunction solar cells, *J. Mater. Chem.*, 2012, **22**(35), 18433–18441.

10 F. Machui, *et al.*, Determination of the P3HT:PCBM solubility parameters via a binary solvent gradient method: Impact of solubility on the photovoltaic performance, *Sol. Energy Mater. Sol. Cells*, 2012, **100**, 138–146.
11 F. Machui, *et al.*, Determination of Solubility Parameters for Organic Semiconductor Formulations, *Macromol. Chem. Phys.*, 2011, **212**(19), 2159–2165.
12 Y. Zhang, *et al.*, Understanding and controlling morphology evolution via DIO plasticization in PffBT4T-2OD/$PC_{71}BM$ devices, *Sci. Rep.*, 2017, **7**, 44269.
13 H.-C. Liao, *et al.*, Additives for morphology control in high-efficiency organic solar cells, *Mater. Today*, 2013, **16**(9), 326–336.
14 M. Shao, *et al.*, Understanding How Processing Additives Tune the Nanoscale Morphology of High Efficiency Organic Photovoltaic Blends: From Casting Solution to Spun-Cast Thin Film, *Adv. Funct. Mater.*, 2014, **24**(42), 6647–6657.
15 S. Das, *et al.*, Correlating high power conversion efficiency of PTB7: PC71 BM inverted organic solar cells with nanoscale structures, *Nanoscale*, 2015, **7**(38), 15576–15583.
16 G. Nichols, *et al.*, A Review of the Terms Agglomerate and Aggregate with a Recommendation for Nomenclature Used in Powder and Particle Characterization, *J. Pharm. Sci.*, 2002, **91**(10), 2103–2109.
17 N. O. McHedlov-Petrossyan, Fullerenes in Liquid Media: An Unsettling Intrusion into the Solution Chemistry, *Chem. Rev.*, 2013, **113**(7), 5149–5193.
18 Q. Ying, J. Marecek and B. Chu, Solution behavior of buckminsterfullerene (C_{60}) in benzene, *J. Chem. Phys.*, 1994, **101**(4), 2665–2672.
19 Q. Ying, J. Marecek and B. Chu, Slow aggregation of buckminsterfullerene (C_{60}) in benzene solution, *Chem. Phys. Lett.*, 1994, **219**(3), 214–218.
20 A. D. Bokare and A. Patnaik, Self-organization of C-60 nanoparticles in carbon disulfide solution, *J. Phys. Chem. B*, 2003, **107**(25), 6079–6086.
21 S. Nath, H. Pal and A. V. Sapre, Effect of solvent polarity on the aggregation of C-60, *Chem. Phys. Lett.*, 2000, **327**(3–4), 143–148.
22 R.-H. Guo, *et al.*, Mesoscale aggregation properties of C_{60} in toluene and chlorobenzene, *Soft Matter*, 2016, **12**(29), 6300–6311.
23 C. I. Wang and C. C. Hua, Solubility of C-60 and PCBM in Organic Solvents, *J. Phys. Chem. B*, 2015, **119**(45), 14496–14504.
24 J. S. Peerless, *et al.*, Fullerenes in Aromatic Solvents: Correlation between Solvation-Shell Structure, Solvate Formation, and Solubility, *J. Phys. Chem. B*, 2015, **119**(49), 15344–15352.
25 D. Boucher and J. Howell, Solubility Characteristics of PCBM and C-60, *J. Phys. Chem. B*, 2016, **120**(44), 11556–11566.
26 J. S. Peerless, *et al.*, Effect of C-60 adducts on the dynamic structure of aromatic solvation shells, *Chem. Phys. Lett.*, 2017, **678**, 79–84.
27 A. D. Bokare and A. Patnaik, C-60 aggregate structure and geometry in nonpolar o-xylene, *J. Phys. Chem. B*, 2005, **109**(1), 87–92.
28 C. M. Hansen and A. L. Smith, Using Hansen solubility parameters to correlate solubility of C-60 fullerene in organic solvents and in polymers, *Carbon*, 2004, **42**(8–9), 1591–1597.
29 K. N. Semenov, *et al.*, Solubility of Light Fullerenes in Organic Solvents, *J. Chem. Eng. Data*, 2010, **55**(1), 13–36.
30 N. O. McHedlov-Petrossyan, *et al.*, The peculiar behavior of fullerene C-60 in mixtures of 'good' and polar solvents: colloidal particles in the toluene-methanol mixtures and some other systems, *Colloids Surf., A*, 2016, **509**, 631–637.
31 R. S. Ruoff, *et al.*, Solubility of fullerene (C_{60}) in a variety of solvents, *J. Phys. Chem.*, 1993, **97**(13), 3379–3383.
32 S. Nath, H. Pal and A. V. Sapre, Effect of solvent polarity on the aggregation of fullerenes: a comparison between C-60 and C-70, *Chem. Phys. Lett.*, 2002, **360**(5–6), 422–428.
33 H. N. Ghosh, A. V. Sapre and J. P. Mittal, Aggregation of C_{70} in Solvent Mixtures, *J. Phys. Chem.*, 1996, **100**(22), 9439–9443.
34 N. Tezuka, *et al.*, Good Solvent Effects of C-70 Cluster Formations and Their Electron-Transporting and Photoelectrochemical Properties, *J. Phys. Chem. B*, 2010, **114**(45), 14287–14297.
35 A. Kaiser, *et al.*, Aggregates of PCBM molecules: a computational study, *Int. J. Mass Spectrom.*, 2014, **365**, 225–231.
36 N. R. Tummala, *et al.*, Effect of Solvent Additives on the Solution Aggregation of Phenyl-C61–Butyl Acid Methyl Ester (PCBM), *Chem. Mater.*, 2015, **27**(24), 8261–8272.
37 S. M. Mortuza and S. Banerjee, Molecular modeling study of agglomeration of 6,6-phenyl-C61-butyric acid methyl ester in solvents, *J. Chem. Phys.*, 2012, **137**(24), 244308.
38 D. T. Duong, *et al.*, Molecular solubility and hansen solubility parameters for the analysis of phase separation in bulk heterojunctions, *J. Polym. Sci., Part B: Polym. Phys.*, 2012, **50**(20), 1405–1413.
39 N. Shin, *et al.*, Effect of Processing Additives on the Solidification of Blade-Coated Polymer/Fullerene Blend Films via In-situ Structure Measurements, *Adv. Energy Mater.*, 2013, **3**(7), 938–948.
40 S. Hu, *et al.*, The impact of selective solvents on the evolution of structure and function in solvent annealed organic photovoltaics, *RSC Adv.*, 2014, **4**(53), 27931–27938.
41 I. Burgues-Ceballos, *et al.*, Solubility Based Identification of Green Solvents for Small Molecule Organic Solar Cells, *Adv. Funct. Mater.*, 2014, **24**(10), 1449–1457.
42 C. M. Liu, *et al.*, Complementary solvent additives tune the orientation of polymer lamellae, reduce the sizes of aggregated fullerene domains, and enhance the performance of bulk heterojunction solar cells, *J. Mater. Chem. A*, 2014, **2**(48), 20760–20769.
43 Y. Xie, *et al.*, Butanedithiol Solvent Additive Extracting Fullerenes from Donor Phase to Improve Performance and Photostability in Polymer Solar Cells, *ACS Appl. Mater. Interfaces*, 2017, **9**(11), 9918–9925.

44 M. J. Hollamby, *et al.*, The aggregation of an alkyl-C-60 derivative as a function of concentration, temperature and solvent type, *Phys. Chem. Chem. Phys.*, 2018, **20**(5), 3373–3380.

45 M. J. Hollamby, *et al.*, Directed assembly of optoelectronically active alkyl–π-conjugated molecules by adding n-alkanes or π-conjugated species, *Nat. Chem.*, 2014, **6**, 690.

46 G. Bernardo, *et al.*, Does 1,8-diiodooctane affect the aggregation state of $PC_{71}BM$ in solution?, *R. Soc. Open Sci.*, 2018, **5**(9), 180937.

47 V. V. Chaban, C. Maciel and E. E. Fileti, Solvent Polarity Considerations Are Unable to Describe Fullerene Solvation Behavior, *J. Phys. Chem. B*, 2014, **118**(12), 3378–3384.

48 J. D. Perea, *et al.*, Combined Computational Approach Based on Density Functional Theory and Artificial Neural Networks for Predicting the Solubility Parameters of Fullerenes, *J. Phys. Chem. B*, 2016, **120**(19), 4431–4438.

49 N. R. Tummala, *et al.*, Packing and Disorder in Substituted Fullerenes, *J. Phys. Chem. C*, 2016, **120**(31), 17242–17250.

50 J. W. Kiel, A. P. R. Eberle and M. E. Mackay, Nanoparticle Agglomeration in Polymer-Based Solar Cells, *Phys. Rev. Lett.*, 2010, **105**(16), 168701.

51 D. Chen, *et al.*, P3HT/PCBM Bulk Heterojunction Organic Photovoltaics: Correlating Efficiency and Morphology, *Nano Lett.*, 2011, **11**(2), 561–567.

52 Y. Zhang, *et al.*, Effect of fullerene acceptor on the performance of solar cells based on PffBT4T-2OD, *Phys. Chem. Chem. Phys.*, 2018, **20**(28), 19023–19029.

53 K. A. Affholter, *et al.*, Structural characterization of C_{60} and C_{70} fullerenes by small-angle neutron scattering, *J. Chem. Phys.*, 1993, **99**(11), 9224–9229.

54 S. J. Henderson, Measurement of the Second Virial Coefficient of C_{60} in CS2 Solution from Small-Angle Neutron Scattering, *Langmuir*, 1997, **13**(23), 6139–6145.

55 M. V. Avdeev, *et al.*, On structural features of fullerene C_{60} dissolved in carbon disulfide: complementary study by small-angle neutron scattering and molecular dynamic simulations, *J. Chem. Phys.*, 2010, **132**(16), 164515.

56 M. V. Avdeev, *et al.*, Structural Features of Molecular-Colloidal Solutions of C_{60} Fullerenes in Water by Small-Angle Neutron Scattering, *Langmuir*, 2004, **20**(11), 4363–4368.

57 M. T. Rekveldt, *et al.*, Spin-echo small angle neutron scattering in Delft, *Rev. Sci. Instrum.*, 2005, **76**(3), 9.

58 H. Gaspar, *et al.*, A Journey along the Extruder with Polystyrene: C_{60} Nanocomposites: Convergence of Feeding Formulations into a Similar Nanomorphology, *Macromolecules*, 2017, **50**(8), 3301–3312.

59 H. Gaspar, *et al.*, Evolution of dispersion in the melt compounding of a model polymer nanocomposite system: a multi-scale study, *Polym. Test.*, 2019, **76**, 109–118.

60 S. R. Parnell, *et al.*, Porosity of silica Stober particles determined by spin-echo small angle neutron scattering, *Soft Matter*, 2016, **12**(21), 4709–4714.

61 S. R. Parnell, G. Bernardo and A. L. Washington, Aggregation effects on long length scales in solutions for organic photovoltaic devices, *STFC ISIS Neutron and Muon Source*, 2018, DOI: 10.5286/ISIS.E.92924123.

62 V. Negi, *et al.*, Simulating Phase Separation during Spin Coating of a Polymer–Fullerene Blend: A Joint Computational and Experimental Investigation, *ACS Appl. Energy Mater.*, 2018, **1**(2), 725–735.

63 A. A. Y. Guilbert and J. T. Cabral, Impact of solution phase behaviour and external fields on thin film morphology: PCBM and RRa-P3HT model system, *Soft Matter*, 2017, **13**(4), 827–835.

64 N. S. Güldal, *et al.*, Real-time evaluation of thin film drying kinetics using an advanced, multi-probe optical setup, *J. Mater. Chem. C*, 2016, **4**(11), 2178–2186.

65 R. Dalgliesh, *Larmor – A flexible instrument for high throughput SANS, Spin-Echo SANS and the development of Larmor precession techniques*, 13th July 2018, available from: https://www.isis.stfc.ac.uk/Pages/Larmor.aspx.

66 C. Bannwarth, S. Ehlert and S. Grimme, GFN2-xTB—An Accurate and Broadly Parametrized Self-Consistent Tight-Binding Quantum Chemical Method with Multipole Electrostatics and Density-Dependent Dispersion Contributions, *J. Chem. Theory Comput.*, 2019, **15**(3), 1652–1671.

67 G. Paterno, *et al.*, Micro-focused X-ray diffraction characterization of high-quality 6,6-phenyl-C-61-butyric acid methyl ester single crystals without solvent impurities, *J. Mater. Chem. C*, 2013, **1**(36), 5619–5623.

68 T. Umeyama, *et al.*, Enantiomerically Separated α-[70]PCBM for Organic Photovoltaics, *Chem. Lett.*, 2017, **46**(7), 1001–1003.

69 M. J. Frisch, *et al.*, *Gaussian 09, Revision D.01*, Gaussian, Inc., Wallingford CT, 2016.

70 A. L. Washington, *et al.*, Inter-particle correlations in a hard-sphere colloidal suspension with polymer additives investigated by Spin Echo Small Angle Neutron Scattering (SESANS), *Soft Matter*, 2014, **10**(17), 3016–3026.

71 S. R. Parnell, *et al.*, Spin echo small angle neutron scattering using a continuously pumped He-3 neutron polarisation analyser, *Rev. Sci. Instrum.*, 2015, **86**(2), 023902.

72 R. Andersson, *et al.*, Analysis of spin-echo small-angle neutron scattering measurements, *J. Appl. Crystallogr.*, 2008, **41**(5), 868–885.

73 P. Debye and A. M. Bueche, Scattering by an Inhomogeneous Solid, *J. Appl. Phys.*, 1949, **20**(6), 518–525.

74 P. Debye, H. R. Anderson Jr and H. Brumberger, Scattering by an Inhomogeneous Solid. II. The Correlation Function and its Application, *J. Appl. Phys.*, 1957, **28**(6), 679–683.

75 E. B. Stukalin, M. V. Korobov and N. V. Avramenko, Solvation Free Energies of the Fullerenes C_{60} and C_{70} in the Framework of Polarizable Continuum Model, *J. Phys. Chem. B*, 2003, **107**(36), 9692–9700.

